Journal of Intelligent Manufacturing
https://doi.org/10.1007/s10845-025-02664-8

Numerical data driven operation support for manufacturing of automotive body components

Alexander Barlo[1] · Omsri Aeddula[1] · Mats Sigvant[1,2] · Johan Pilthammar[1,3] · Toni Chezan[4] · Md Shafiqul Islam[1] · Tobias Larsson[1]

Received: 12 November 2024 / Accepted: 16 July 2025

Abstract
With the increased focus on smart manufacturing and Industry 4.0, the use of simulations for the creation of cyber-physical manufacturing systems is increasing. The sheet metal forming manufacturing process, commonly used for production of automotive body components, is one of the processes that currently benefits from the use of simulations without exploiting them in a cyber-physical system setup. This study set out to initially identify the key controllable and uncontrollable parameters of the sheet metal forming manufacturing process for the design of an intelligent quality controller. Subsequently, the study investigates the possibility of using data points from a stochastic numerical analysis as training data for an Artificial Neural Network. The stochastic numerical model used is based on the existing Finite Element simulation standard at Volvo Cars to allow for a seamless integration of the methodology into the standard workflow of CAE departments. Lastly, the study will present a validation of the trained Artificial Neural Network using the Volvo XC90 inner front door component as an industrial demonstrator.

Keywords Artificial neural network · Deep drawing · Process control · Virtual shadow · Industry 4.0

Introduction

The use of simulation for the creation of cyber-physical manufacturing systems has rapidly increased over recent years (Yu & Nielsen, 2020; Jeong et al., 2020; Sbaragli et al., 2025). The main driver for use of the virtual space in collaboration with the physical is manufacturing companies embracing the philosophies of Industry 4.0 (Germany), Smart Manufacturing (USA) or Made in China 2025 (China) (Maier et al., 2024; Tao et al., 2018). Common for the three philosophies is, amongst other, the desire to establish a seamless integration between the the virtual and physical world in the framework of Digital Twins (DT) and Cyber-Physical Systems (CPS) (Semeraro et al., 2021). One way to achieve this is through the utilization of advances in sensor technology and data storage together with the introduction of Artificial Intelligence (AI) and the Internet of Things (IoT) (Singer & Cohen, 2021). These new technologies have set the stage for the introduction of intelligent quality controllers in a manufacturing setup.

The manufacturing process of deep drawing is widely used in industry with applications in automotive, aerospace, household appliances, and consumer electronics. According

Alexander Barlo and Omsri Aeddula have contributed equally to this work.

✉ Alexander Barlo
Alexander.Barlo@bth.se

Omsri Aeddula
Omsri.Kumar.Aeddula@bth.se

Mats Sigvant
Mats.Sigvant@autoform.com

Johan Pilthammar
Johan.Pilthammar@volvocars.com

Toni Chezan
Toni.Chezan@tatasteeleurope.com

Md Shafiqul Islam
Shafiqul.Islam@bth.se

Tobias Larsson
Tobias.Larsson@bth.se

[1] Blekinge Institute of Technology, Karlskrona, Sweden

[2] AutoForm Engineering AB, Olofström, Sweden

[3] Volvo Cars, Olofström, Sweden

[4] TATA Steel Europe, IJmuiden, The Netherlands

Published online: 01 August 2025

to the DIN (2003) standard, deep drawing is classified as a subcategory under the DIN 8584 class *forming under compressive and tensile conditions*. While the process might seem simple, the underlying mechanics are not. When performing a deep drawing operation, one must consider the theory of large deformations, large strains and elasto-plastic material behavior (Banabic, 2010), all highly non-linear by nature. In the automotive industry, the deep drawing process is used for the manufacturing of body components such as doors, wheelhouses and fenders. As the competition for market share within the automotive industry increases, so does the demand from customers on topics such as styling, safety and sustainability. Increased component complexity, and demands to introduce sustainable materials (such as secondary steel and aluminum grades) increases the difficulty of the deep drawing operation as robust process windows will become increasingly more difficult to determine. Especially the introduction of secondary materials is expected to introduce a higher level of in-production variation of material properties. The standard practice today is that a single set of material parameters describes the entire coil. With the introduction of secondary, scrap-based materials, this assumption may no longer be valid, making the deep drawing operation more volatile and uncertain. A way to counteract this increased volatility is through the use of digital tools for support and decision making on the production floor.

This paper will investigate the possibilities for the development of an intelligent quality controller for the deep drawing manufacturing process. The paper aims to train an Artificial Neural Network (ANN) using numerically generated data for an industrial demonstrator component; the Volvo XC90 front door inner component, manufactured from a VDA239 CR4 mild steel.

State-of-the-art review

The use of data-driven methods for the improvement of the deep drawing process has seen an increase in interest in recent years. Link et al. (2025) presents a study on the development of a digital twin for real-time quality prediction and local adjustment of friction in deep drawing. In this study a Convolutional Neural Network (CNN) was applied to a double-symmetric part of DC01 steel to model the correlation between the friction conditions and blankholder force (BHF) to the final part geometry and thinning of the formed part. The study used synthetic training data generated through Finite Element simulations to train the CNN. Similarly, Gou et al. (2025) applied a Deep Neural Network (DNN), also trained on synthetic data, on a cylindrical cup of SPCC steel to predict the thickness of the sheet in six locations, based on the blankholder force (BHF), the radius of the punch, and the temperature. Hou and Behdinan (2025) also investigated the cylindrical cup, using a dimensionality-reduced neural network (DR-NN). In this study, various aspects of tool geometry and material parameters were used as features of the network to predict the flange springback. Similarly, Morand et al. (2019) used Random Forrest Classification and Gaussian Process Regression to predict geometrical features of the cylindrical cup of DP600 dual-phase steel. The study used synthetic training data generated from Finite Element simulations using a Hill'48 anisotropic yield criterion calibrated from experiments.

Guo and Yu (2019) presented a framework deploying a reinforcement learning algorithm to control the blankholder force during the forming of a similar cylindrical cup of low carbon steel using an actor-critic approach.

Studies by Thiery et al. (2024) and Wollschlaeger et al. (2024) investigated data-driven approaches on the more complex shape known as the cross-die. Both studies investigated how data driven methods (Artificial Neural Networks and Transfer Learning respectively) can increase the reliability of draw-in predictions using either fully synthetic or hybrid training data strategies. Lehrer et al. (2023) used a similar cross-die geometry to develop a method for enhancing the efficiency and accuracy of drawability assessments. The study presented a combination of classification models, to distinguish between drawable and non-drawable setups, with regression models to rank designs by drawability. The study used a combination of low and high-fidelity Finite Element simulations to generate synthetic training data.

Motivation, novelty and method

Although the studies presented in the State-of-the-Art review have displayed various degrees of successful implementation of data-driven methods for deep drawing, this has been done under controlled and ideal process conditions for components of relative low complexity. As a result, they are unable to capture the complex variations found in fully operational manufacturing processes of automotive body components.

The following study aims to present a Proof-of-Concept (PoC) showing that data-driven quality controllers for industrial use can be trained using synthetically generated data. The study will be based on a two-stage methodology, where stage one will focus on data generation, while stage two will handle the final model training.

During the data generation stage, a detailed analysis of the manufacturing system for the industrial demonstrator will be presented identifying key process variables and process responses along with the identification of features and targets for the Artificial Neural Network. In the following step, empirical data will be used to identify the ranges

of in-process variations that can be expected for the given industrial demonstrator. These ranges will simultaneously serve as the upper and lower boundaries of parameter variation for a stochastic Finite Element model used to generate synthetic training data. In this stage, the study will also present how a high-fidelity Finite Element model of the industrial deep drawing process can be developed using advanced material models, tribology models, and recorded knowledge on machine kinematics.

In the model training stage, the study will present the data pre-processing approach to prepare the synthetic data for the learning algorithm. In this stage, the model architecture will also be presented along with information on hyperparameter tuning. Finally, the study will present how the model performs when exposed to real production data from the production facility at Volvo Cars. An outline of the methodology with all steps is presented in Fig. 1.

Industrial testbed

The industrial testbed used in this study consists of an industrial press line and an industrial blanking line. Both industrial lines are located in the production facilities of Volvo Cars in Olofström, Sweden. The press line is a 2D-transfer line using one forming station, with a maximum available tonnage of 1000 tons, and multiple stations for subsequent operations. A standard blanking line is used to trim the blanks from the coil.

In an effort to gain more insight into the manufacturing process, sensors have been placed at several locations both in the blanking and press line. The technical specifications of each sensor will not be presented in this study, as these are at the time of writing considered sensitive information by Volvo Cars. A generic description of some key sensors along with the overall data flow will however be presented.

In order to achieve full traceability of the blanks throughout the manufacturing process (and subsequent assembly process) a system is in place correlating each blank to a specific location on a specific coil of material. The specific coil information from the supplier is stored from the material certificate, containing information such as material properties (including initial yield stress, tensile strength, and anisotropy coefficient), coating levels, and surface roughness of the sheet. In the blanking line, a laser-based measurement system is also placed to measure the lubrication distribution on both the top and bottom side of the blank.

In the press line, several force channels are monitored, the two most important being the cushion and the ram force. Both these force channels are recorded during the press stroke and linked to a specific blank in the Data Acquisition (DAQ) system. Since the press consist of mechanical presses with flywheels, the crank angle is recorded to monitor the ram position at all time during the stroke. The described sensor setup is summarized in Table 1, and the data flow to a central database is illustrated in Fig. 2.

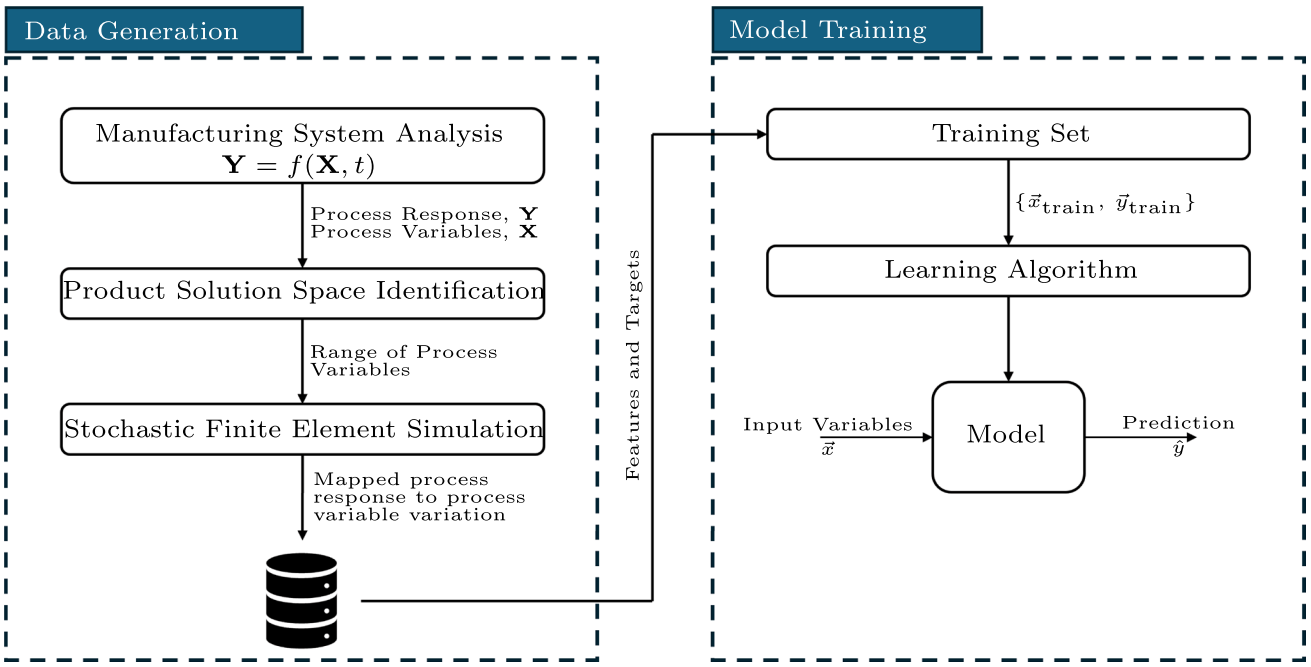

Fig. 1 Two-stage methodology employed in the study to develop the Proof-of-Concept for an industrial intelligent quality controller

Table 1 Overview of sensors and sampling frequencies for key sensors implemented in the industrial testbed

Measurement type	Target	Location	Sampling frequency
Force measurement	Cushion force	Press	$\sim$ 52 [Hz]
Force measurement	Ram force	Press	$\sim$ 52 [Hz]
Position measurement	Crank angle	Press	$\sim$ 52 [Hz]
Oil Film measurement	Lubrication amount	Blanking line	$\sim$ 17 [Hz]
Position measurement	Strip position	Blanking line	–

Manufacturing system analysis

To design an intelligent quality controller for any manufacturing system, three features need to be included: (1) an ability to track changes in process response characteristics with time, (2) an ability to monitor uncontrollable variables, and (3) an ability to perform real-time process parameter design (Chinnam & Kolarik, 1997). This can be expressed mathematically in the following form:

$$\mathrm{Y} = f(\mathrm{X}, t) \tag{1}$$

where Y is the process response characteristics of interest, organized in a column vector such that

$$\mathrm{Y} = [Y_1, \ldots, Y_N]^T$$

X is the process variables organized in a column vector such that

$$\mathrm{X} = [X_1, \ldots, X_K, X_{K+1}, \ldots, X_M]^T$$

with K controllable variables (X_1 through X_K), and $M - K$ uncontrollable variables (X_{K+1} through X_M), and t representing the operation time, making the system time-variant.

Manufacturing process layout

For most automotive deep drawing operations, multiple steps are involved in transforming the flat metal sheet into the final desired shape. For the industrial demonstrator component in this study, a total of five forming operations are performed, denoted OP 10–60. Initially, the OP 10 stage describes the blanking operation, where the initial blank geometry of the component is separated from a larger coil of sheet metal. The second stage, OP 20, is where the majority of the forming occurs, meaning almost of all of the geometry is in place after this step. For the given demonstrator component, OP 30–60 are trimming operations where excess material is removed from the component to achieve the desired final geometry. The geometry of the component at the different stages of the process can be seen in Fig. 3. From this point, when referring to the manufacturing process of the demonstrator component, this will refer to the OP 20 stage.

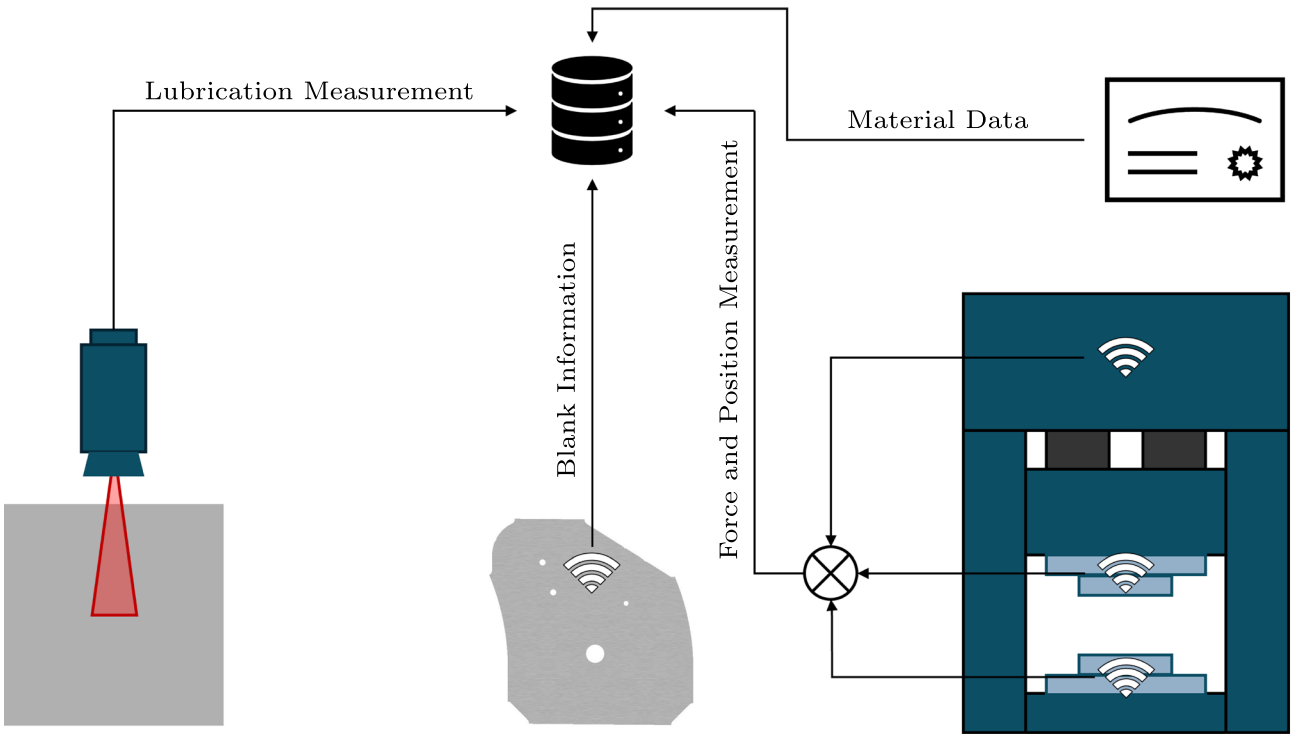

Fig. 2 Data flow of implemented Data Acquisition System in the industrial testbed

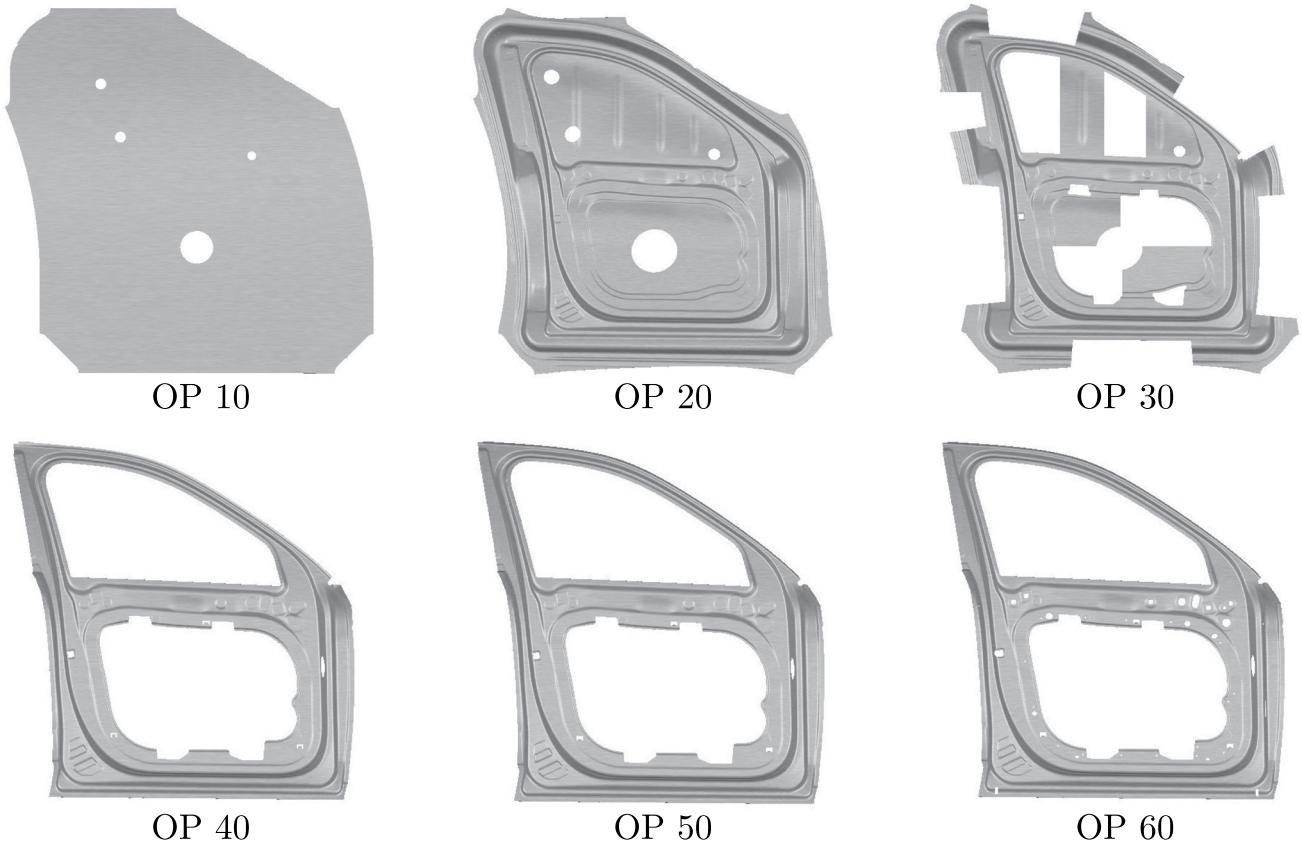

Fig. 3 Steps of the sheet metal forming process to manufacture the Volvo XC90 inner front door component

Process response characteristics

As presented in Eq. 1, the control response characteristics takes the form of the unique solution to the equation. Therefore, the control response characteristic must be a somehow quantifiable parameter. For the chosen demonstrator only the first drawing operation is considered. This limits the amount of response parameters to the sheet draw-in ζ, and the sheet springback ϑ. Practically, performing an in-line measurement of the sheet springback is challenging, as the measurements must be performed while the part is still stationary in the die to achieve the most accurate results. Integrating sensors into the die structure is a way to achieve this as proposed by Maier et al. (2017), but in the case of the chosen demonstrator this would require modifications to a production die. Methods for in-line measurements of draw-in on the other hand, have previously been proposed by several authors (Tricarico & Palmieri, 2023; Amirgol, 2022) requiring no modifications to the existing die.

For the determination of the sheet draw-in, a reference point is needed. In the case of the chosen demonstrator, the trapped blank outline is selected, to exclude the draw-in caused by the draw bead forming. The sheet draw-in is however not a single global parameter, why several measurement points on the trapped blank must be chosen. In the present study, 15 points are defined as presented in Fig. 4, causing the following form of the process response characteristics column vector:

$$\mathrm{Y} = [\zeta_1, \ldots, \zeta_{15}]^T$$

Controllable and uncontrollable variables

For the modeling of the different variables of the process, one must distinguish between controllable (X_K) and uncontrollable variables (X_{M-K}). The variables are compartmentalized depending on weather they can be influenced by external factors during the process i.e. controllable variables can be adjusted during the process by operators or engineers, whereas uncontrollable variables can not.

For the sheet metal forming process, a variety of variables exists that needs to be considered - all interacting with each other. These parameters and their interactions have previously been mapped by Sigvant et al. (2018) with the purpose of improving Finite Element (FE) modelling. This mapping is presented in Fig. 5. Since the discipline of FE modelling targets to create a virtual replica of the forming

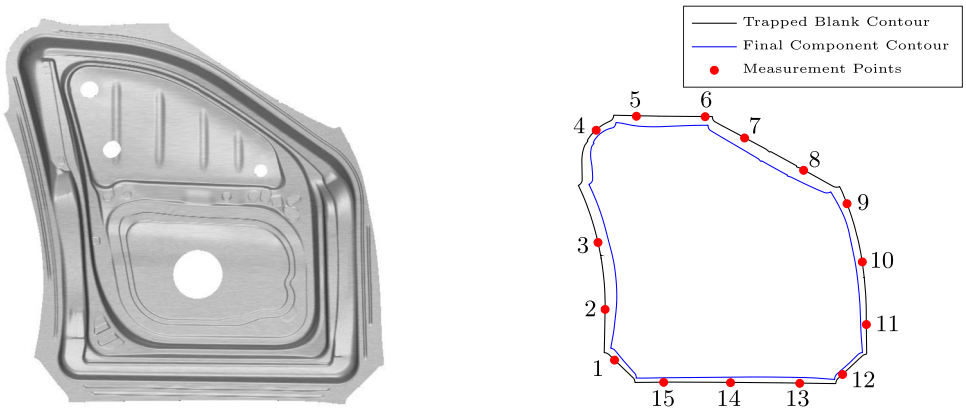

Fig. 4 Volvo XC90 Front Door (left), and illustration of trapped blank and final component contours displayed with the 15 measurement points used in the study (right)

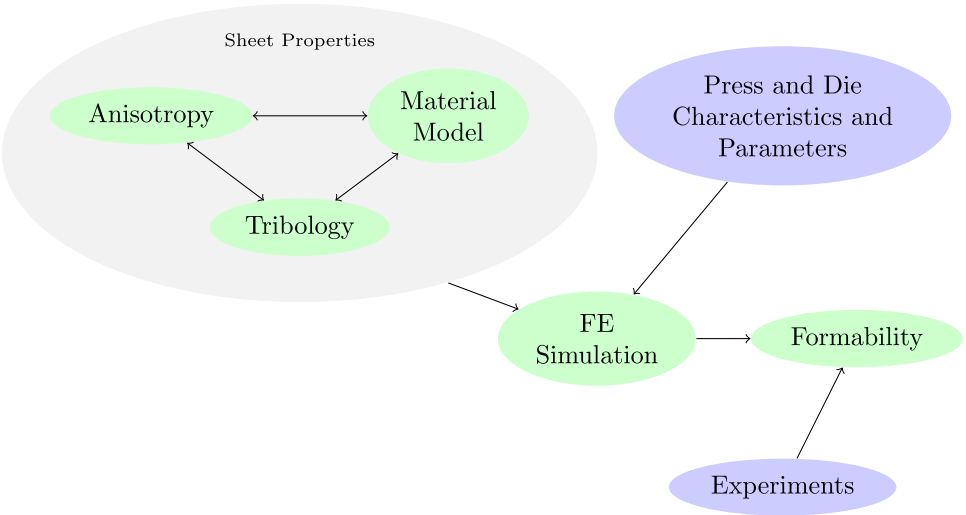

Fig. 5 Interaction between different variables identified by Sigvant et al. (2018)

process, the variables presented in this work will form the basis for the determination of controllable and uncontrollable variables in this study.

Starting with the sheet properties three main groups are considered; Anisotropy, Tribology, and Material Model. As the Material Model group relates exclusively to modelling, this will be replaced by the group Material Parameters which relates more to the physical sheet.

Anisotropic material behaviour of the sheet is an expression for the material having different mechanical properties in different directions. The anisotropic behaviour occurs due to the rolling process at the steel mill transforming a metal slab to a flat sheet, why it must be considered an *uncontrollable* variable for the stamping plant. In reality three different variables describes the anisotropic behavior of metallic sheets, called Lankford Coefficients (R). These coefficients are taken in three directions to the rolling direction of the sheet: 0º, 45º, and 90º. However, according to Hosford and Caddell (2007) it is customary to define an average value ($\bar{R}$) as:

$$\bar{R} = \frac{R_0 + 2R_{45} + R_{90}}{4}$$

Tribology covers, amongst other, the friction behaviour between the sheet and tool. Historically, friction has been modelled using the static Coulomb friction model, however in reality, the friction behaviour is dependent on contact pressure, sliding velocity, straining, and contact surface temperature as described by Hol et al. (Hol et al., 2012, 2017). To model this dynamic friction behaviour for real-world applications, the type of lubricant and amount of lubrication (ϱ) that is applied to the sheet is of interest. The sheet comes with an amount of lubrication from e.g. the steel mill for corrosion protection, but the operators have the opportunity to add lubrication in troublesome spots, making it a *controllable* variable.

For the material parameters, two variables are interesting; the initial yield stress σ_0, and the tensile strength σ_m. For the sheet metal forming process, the goal is to plastically deform the sheet into a final geometry, why the initial yield point can have quite an impact on the process. The tensile strength is considered due to its relation to the yield stress. In a stamping operation, the component will ideally

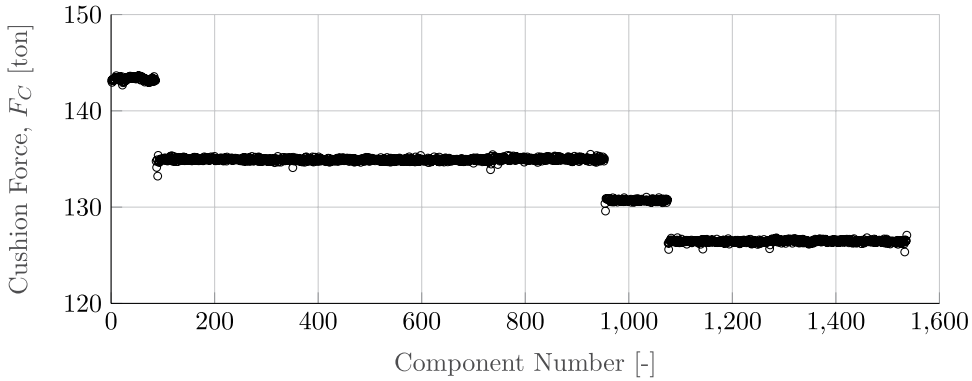

Fig. 6 Cushion force F_C tracked over a batch of 1564 front door inner components in running production

Table 2 Classification of controllable and uncontrollable variables for the sheet metal forming process

Variable type	Variable	Symbol	Unit
Controllable	Cushion force	F_C	ton
	Lubrication amount	ϱ	g/m^2
Uncontrollable	Initial yield stress	σ_0	MPa
	Tensile stress	σ_m	MPa
	Avg. lankford coefficient	$\bar{R}$	–
	Temperature[1]	T	ºC

[1] Time-variant variable

not reach this limit, since this would mean it passes the point of necking, thereby making it a non-conforming part. Therefore, to model accurate physical behavior this parameter must be taken into account. Both of these variables are determined during the creation of the steel sheet, why both will be classified as *uncontrollable* variables.

Lastly, for the tooling and press line variables, the main variable that is considered is the Cushion Force F_C. This is the main variable the operators adjust during running production if the formed component should not meet quality standards. Figure 6 present measurements from a full batch of 1564 components where it can be seen that at least three large adjustments to the cushion force has been made over time. Therefore, the Cushion Force F_C is a *controllable* variable. One reason there is a need for the constant adjustment of the cushion force, is due to the temperature development in the tooling created by heat transfer from the sheet formed during the plastic work. Temperature T has been proven to have an impact on product quality, especially through changes in friction (Waanders et al., 2020; Kott et al., 2020; Barlo et al., 2024b), why this must be considered a time-variant *uncontrollable* variable.

With all variable classified, Table 2 summarises and presents the controllable and uncontrollable variables of the sheet metal forming process.

Creating the column vectors for the controllable and uncontrollable variables we get:

$$\mathrm{X}_K = [F_C \quad \varrho]^T \qquad \text{and} \qquad \mathrm{X}_{M-K} = [\sigma_0 \quad \sigma_m \quad \bar{R} \quad T(t)]^T$$

resulting in a full process variable column vector X

$$\mathrm{X} = [\mathrm{X}_K \quad \mathrm{X}_{M-K}]^T = \left[F_C \quad \varrho \quad \sigma_0 \quad \sigma_m \quad \bar{R} \quad T(t)\right]^T$$

Real time process parameter design

Sections 2.2 and 2.3 mapped the process response characteristics (Y) and process variables (X) respectively. Combining these in the format of Eq. 1 one get:

$$\begin{bmatrix} \zeta_1 \\ \vdots \\ \zeta_{15} \end{bmatrix} = f\left(\left[F_C \quad \varrho \quad \sigma_0 \quad \sigma_m \quad \bar{R} \quad T(t)\right]^T\right)$$

For the design of an intelligent quality controller, one must identify one or multiple process variables that will become the main variable(s) to control during the process. As highlighted in Sect. 2.3, the cushion force F_C is frequently adjusted over a full batch. At Volvo Cars this is currently done manually by the operators, based on experience earned over several years of employment. Therefore, the cushion force is an optimal candidate to be the real time process parameter for the sheet metal forming process. Previous studies have explored the possibility of active blankholder control through the use of actuators (Brun et al., 2021; Simonetto et al., 2023) or hydraulic systems (Tommerup & Endelt, 2012). These options does however require extensive modifications to the existing dies, why they will not be considered in this study. The other candidate is the lubrication amount ϱ, but the frequency of which spot lubrication is added to the blank is far less than how often the cushion force is changed. In addition, not all production lines are equipped with a re-oiler thereby for some cases making the lubrication amount an uncontrollable variable. Therefore, the final expression for the real-time process parameter looks the following:

$$F_C = f\left([\zeta \quad \varrho \quad \sigma_0 \quad \sigma_m \quad \bar{R} \quad T(t)]^T\right) \tag{2}$$

where

$$\boldsymbol{\zeta} = [\zeta_1, \ldots, \zeta_{15}]^T$$

Stochastic numerical model

For the training of the neural network, numerical data will be used. Stochastic numerical models have in earlier studies (Barlo et al., 2024a; Maier et al., 2024; Pareek et al., 2025) proven to be a cheap and fast way to generate training data for neural networks. For this study, the numerical model has been set up in the commercial Finite Element software AutoForm utilizing the Sigma plug-in to emulate expected fluctuations of the controllable and uncontrollable variables of the process.

Base model

The chosen industrial demonstrator has together with a similar component (rear inner door from the same car) been the subject of numerous scientific studies in the past. In-depth studies on the modeling of the tribological system (Sigvant et al., 2016, 2018, 2019; Tatipala et al., 2018a, b), process modeling (Sigvant et al., 2018; Tatipala et al., 2018a; Chezan et al., 2023, 2024), material modeling (Pilthammar et al., 2021), and tool modeling (Sigvant et al., 2018; Pilthammar et al., 2018, 2019) have been published, emphasizing the effort made over time to have an accurate numerical model of a complex industrial component. The modeling of the base model in this study will build on the knowledge gained in the previous studies.

When creating a numerical model for simulating deep drawing operations, the choice of constitutive model strongly influences the accuracy of the model (Banabic & Sester, 2012). For the numerical model in this study the Vegter 2017 constitutive model was chosen due to its ability to be calibrated utilizing only tensile test data, and with a similar accuracy to commonly used constitutive models such as Barlat YLD2K and BBC2005 (Abspoel et al., 2017). A different version of the constitutive model exists - the Full Vegter constitutive model, however, according to Atzema et al. (2021) "*...the mechanical experiments for full Vegter are difficult to carry out correctly and it is highly likely that the Vegter 2017 is more accurately describing the material than a measured full Vegter, because it is averaged over so many materials that test noise becomes negligible.*". Therefore, the use of the Vegter 2017 constitutive model is considered justified.

The press kinematics is modelled to follow the motion curve of the real press, and a stroke rate of 14 [1/min] was used. This stroke rate has an impact on how the hardening behaviour of the material is modelled, as a single hardening curve obtained from quasi-static material testing is deemed to not be sufficient. Therefore, strain rate sensitive hardening curves, with rates ranging from 1×10^{-9} to 100 [s^{-1}] was utilized. For the VDA239 CR4 mild steel, these strain rate sensitive hardening curves were obtained from the Aurora® Online database by TATA Steel Europe (TATA Steel Europe, 2025). The strain rate sensitive hardening curves and yield surface of the Vegter 2017 constitutive model can be seen in Figs. 7 and 8 respectively.

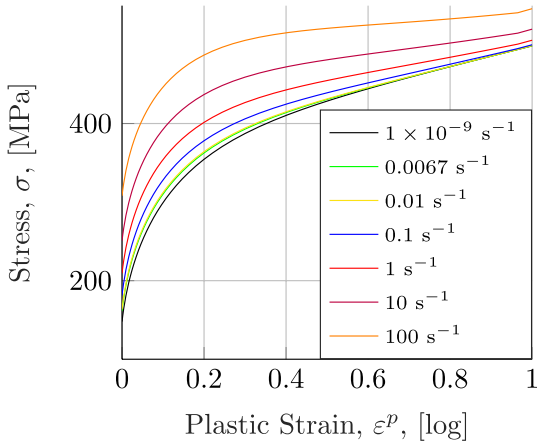

Fig. 7 Strain rate sensitive hardening curves of the VDA239-CR4 mild steel

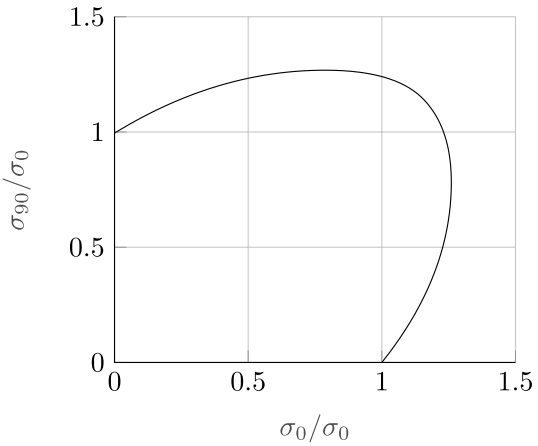

Fig. 8 Yield surface of the VDA239-CR4 mild steel defined through the Vegter2017 constitutive model

The tool surfaces used have been obtained from scan data as opposed to CAD geometries, to account for corrections made during the physical tool tryout to ensure a robust process (Pilthammar, 2020). Having scan data of the tool surfaces subsequently allows for a more accurate modelling of the tribology in the process (Fig. 9(left)). As one of the controllable variables of the process identified was the lubrication amount, tribology is not modelled using the standard

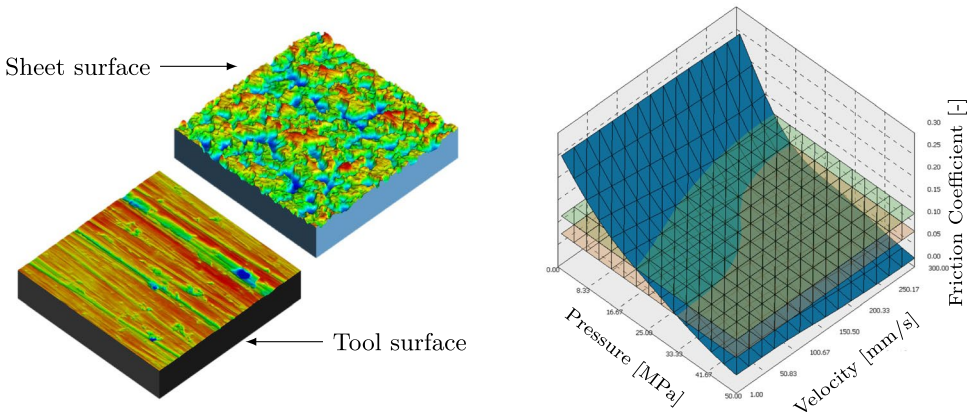

Fig. 9 Tribology system used for the base model. Illustration of the sheet and tool surfaces (left), and a comparison of the TriboForm friction coefficient as a function of pressure and velocity (blue) and standard Coulomb friction (green/orange) (right)

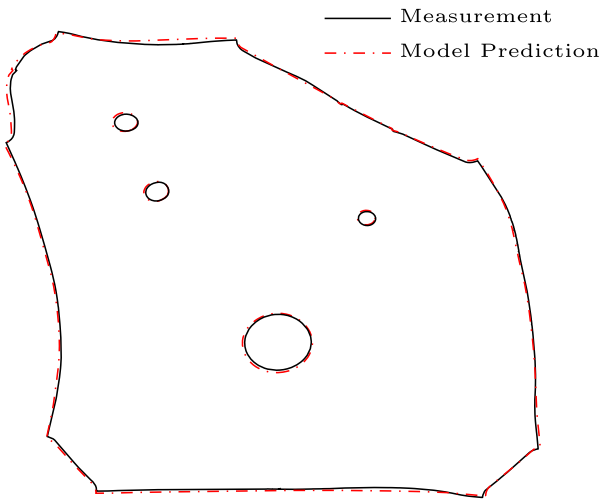

Fig. 10 Comparison of scanned and predicted blank outlines. The scanned outline is obtained using the HandySCAN 700 from Creaform

Coulomb friction model, but through the TriboForm® plug-in to AutoForm. In this plug-in a friction coefficient is provided per element per time step, with the coefficient determined based on contact pressure, sheet velocity, strain levels, and contact surface temperature. This significantly increases resemblance of the real situation compered to previous studies, e.g. Sigvant and Carleer (2006) where a global friction coefficient was varied between 0.008 and 0.12. A comparison of the TriboForm surface and the Coulomb friction coefficients used by Sigvant & Carleer can be found in Fig. 9(right).

Base model validation

To justify the use of the presented base model as a foundation for the generation of training data, a validation of the model is performed using experimentally obtained data.

In the industrial testbed, a grid-pattern was etched onto an undeformed blank, and a lubrication amount of 1 [g/m^2] was manually applied. The prepared blank was placed in the stack, and the press line was run in single-stroke mode with a cushion force of 1500 kN. The drawn panel was then manually extracted, and was immediately scanned, using the HandySCAN 700 from Creaform. Using the scanned geometry, an evaluation on the accuracy of the models ability to predict geometry can be made. Figure 10 presents a comparison of the scanned blank outline and the blank outlines as predicted by the calibrated base model. The figure illustrates a satisfying prediction of the scanned outline, partially validating the calibrated based model from a geometrical point-of-view.

To fully validate models ability to predict the drawn geometry, the etched grid-pattern is analyzed using ARAMIS XL. In order to compare ARAMIS XL data to the model prediction, the deviation Δx is determined as:

$$\Delta x = x_{\text{measured}} - x_{\text{predicted}} \tag{3}$$

where x_{measured} is the result obtained with ARAMIS XL, and $x_{\text{predicted}}$ is the model prediction. Figure 11 presents a fringe plot of the geometrical deviation Δz. The comparison shows an overall low deviation between the measured and predicted geometry values, further validating the model from a geometrical point-of-view.

In deep drawing, a measure that is frequently used to assess the accuracy of a model is the principal strains, due to their application in the Forming Limit Diagram. Figure 12a and b presents the measured and predicted strains along with the calculated deviation for the major and minor principal strain respectively. The comparison shows a good prediction of the principal strains, however with small deviations seen around the apertures in the component.

With the presented comparison of measurements and model prediction of both geometry and strains, the calibrated base model is considered validated as a useful model for the generation of training data.

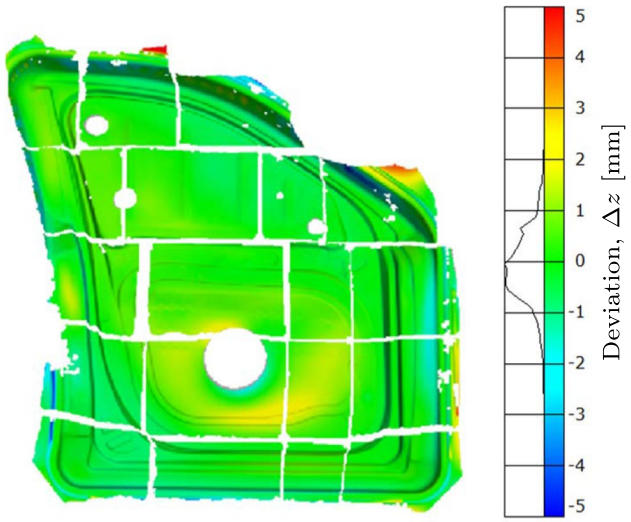

Fig. 11 Comparison of measured and predicted geometry. The fringe plot presents the deviation between measured and predicted z-coordinate

Solution space

With the base of the model defined, the solution space for the stochastic part can be set up. The solution space contains the controllable and uncontrollable variables identified for the process, and upper and lower bounds for the variation must be defined as well as any known relations between parameters.

Bounds of solution space

For the mechanical properties of the mild steel used for the component, these are a result of the sheet coil manufacturing process at the steel mills. When delivering mild steel grades, manufacturers follow a standard for classification of the material grade dictating upper and lower bounds for the mechanical properties. For the CR4 mild steel used in this study, the VDA 239-100 standard (Verband, 2024) is followed, why the upper and lower bounds from this standard is used as a delimiter for the solution space. The determined minimum and maximum values for the material parameters can be found in Table 3.

For determining the bounds of the process parameters, a more practical approach was adopted. For the cushion force, the measurements presented in Fig. 6 was used as an initial guideline for the range. Standard Finite Element simulations were run with a cushion force of 1200 and 1800 kN to ensure that the selected bounds did not result in failure, splits, or wrinkles in the component. As both levels of cushion force proved to produce a safe component, these values were chosen to be the upper and lower bound of the solution space.

For the range of the lubrication Muñiz et al. (2023) investigated a DC06 cold rolled mild steel, an equivalent to the CR4 mild steel investigated in this study. For an industrial example, lubrication amounts of 1, 2.4, and 4 [g/m^2] were reported. For a similar study Sigvant et al. (2019) identified an average lubrication value of 2 [g/m^2] for an industrial component of the same CR4 mild steel grade as investigated in this study. From experience the upper limit of the study by Muñiz et al. is too high for the given industrial demonstrator, however the lower limit is considered reasonable. Given the presented literature, a lubrication range of 1.0–2.0 [g/m^2] will be used in this study.

Capturing the effects of temperature changes during the process is a difficult task to perform numerically, and even more troublesome to capture in reality. Therefore, for the presented study, the temperature effects outlined earlier in Sect. 2.3 have been chosen to be left out.

$$\begin{bmatrix} \zeta_1 \\ \vdots \\ \zeta_{15} \end{bmatrix} = f\left(\begin{bmatrix} F_C & \varrho & \sigma_0 & \sigma_m & \bar{R} \end{bmatrix}^T \right) \tag{4}$$

Mapping of variable relations

To ensure that the neural network is trained on data that is rooted in reality, physics-based relations between variables must be considered in the stochastic model. Figure 13a–c outlines the relationships between the three material parameters, and Fig. 13d presents the relationship between the two process parameters. For the relationship between the initial yield stress and the tensile stress (Fig. 13a), an 85% positive interaction is assumed to ensure that an increase in initial yield stress will not result in a decrease in tensile stress. For the interaction between the other parameters, no physics-based constraints are introduced, but a strong focus on covering the entire solutions space was held.

Output

The stochastic simulation was set up to run 470 realizations, creating a suitable number of data points for training the neural network (Smolic, 2024). From simulation, the draw-in, measured perpendicularly from the trapped blank, was extracted for each of the 15 measurement points. Examples for all extracted draw-in measurements can be seen for four measurement points in Fig. 14.

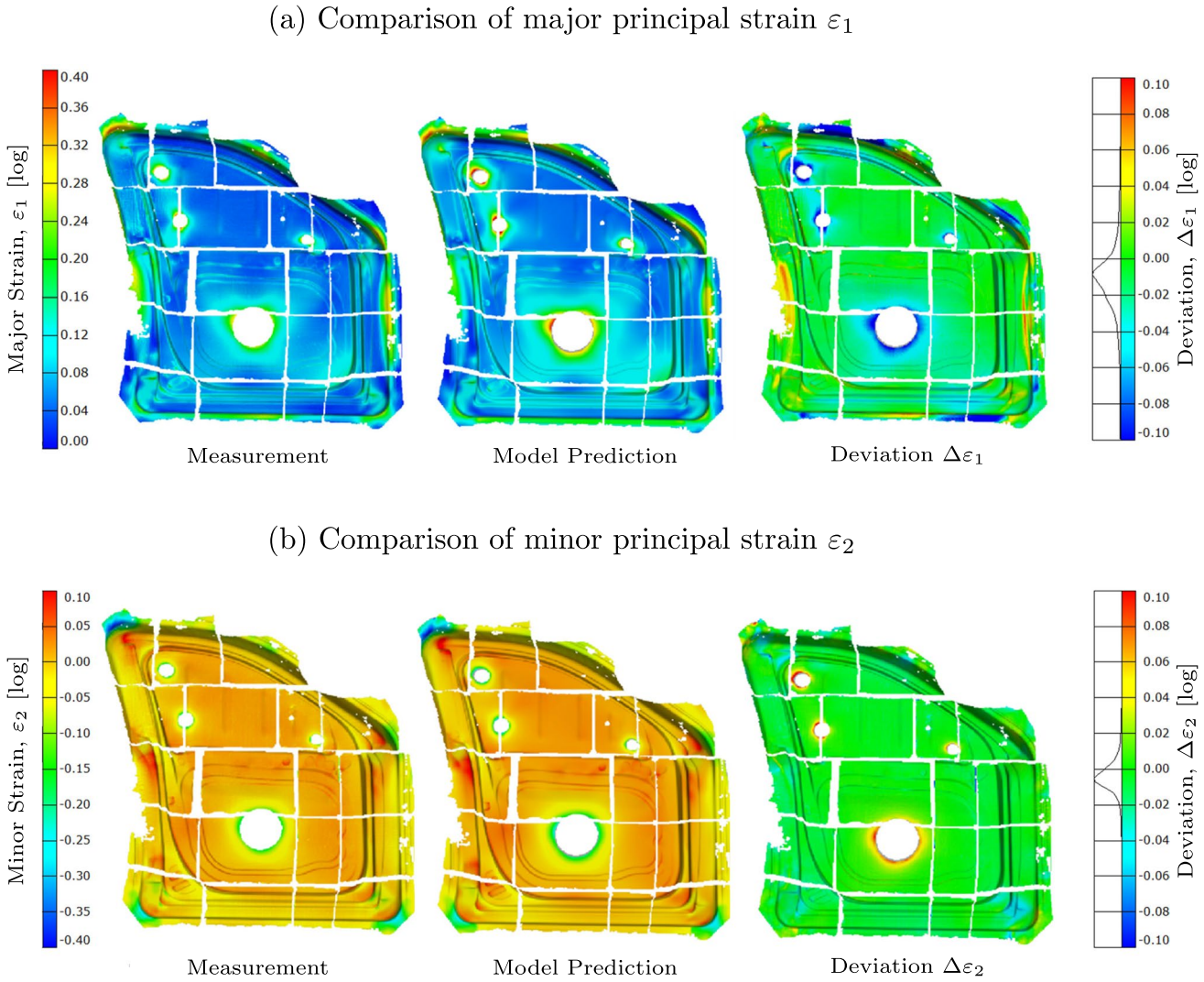

Fig. 12 Comparison of measured and predicted principal strains for the industrial demonstrator drawn with a cushion force of 1500 kN

Table 3 Solution space defined for the stochastic numerical model

Variable	Min	Avg.	Max	σ
Initial yield stress (σ_0) [MPa]	140	160	180	± 20
Tensile strength (σ_m) [MPa]	270	300	330	± 30
Avg. lankford coefficient ($\bar{R}$) [-]	1.6	2.1	2.6	± 0.5
Lubrication amount (ϱ) [g/m^2]	1.0	1.5	2.0	± 0.5
Cushion force (F_C) [kN]	1200	1500	1800	± 300

Neural network design and training

Accuracy of the intelligent quality controller is essential when dealing with a high volume manufacturing process. Previous studies (Barlo et al., 2024a; Witten et al., 2011) have shown how neural networks excel at learning complex patterns from intricate, multi-faceted data, making them ideal for tackling real-world problems. The research in this paper will therefore focus on designing a multi-layer neural network optimized for the real time process parameter identified in Sect. 2.4—the cushion force.

Network architecture

The neural network architecture critically impacts model performance. In this study, a fully connected feed-forward network is employed to capture the complex relationships between input and output data, enabling accurate predictions on unseen data. To enhance model performance and generalization, the network architecture was designed with three hidden layers. The decision to implement this specific architecture was based on empirical evaluations of various configurations, balancing accuracy and computational efficiency. The neural network architecture consists of three key elements; an input layer, hidden layers, and an output layer:

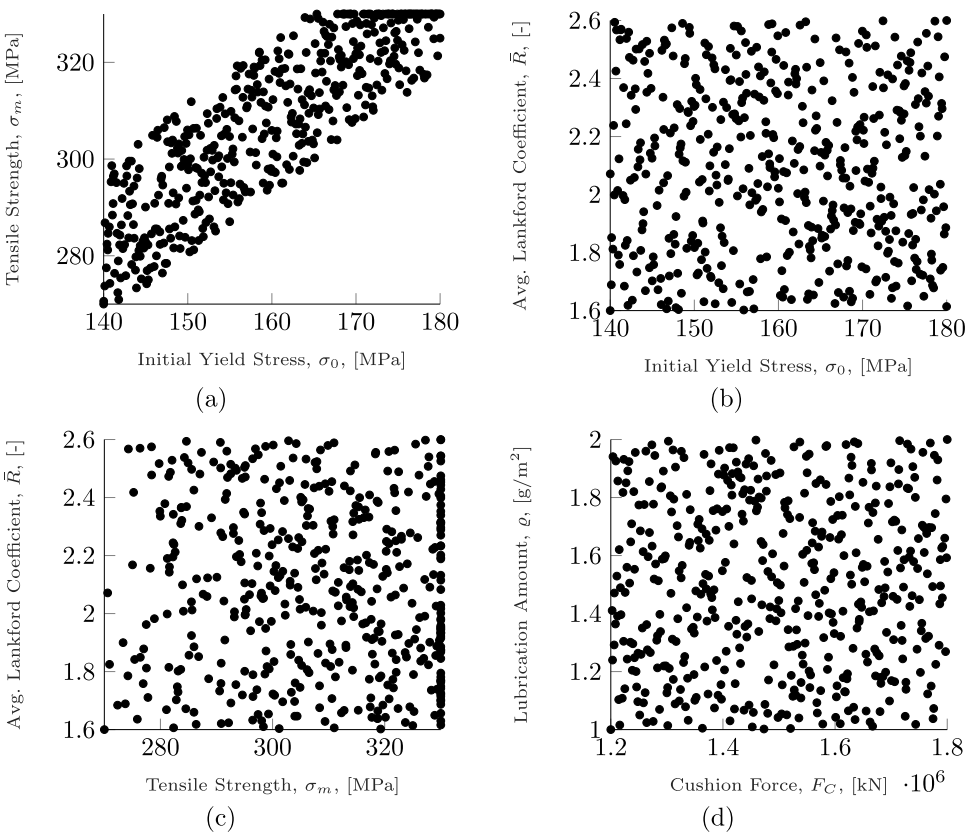

Fig. 13 Relationships between mechanical properties of the VDA239 CR4 mild steel; relationship between (**a**) initial yield stress σ_0 and tensile stress σ_m with an assumption of 85% positive interaction, **b** initial yield stress σ_0 and average Lankford coefficient $\bar{R}$, and **c** tensile stress σ_m and average Lankford coefficient $\bar{R}$. Relationship between process parameters; relationship between **d** cushion force F_C and lubrication amount ϱ

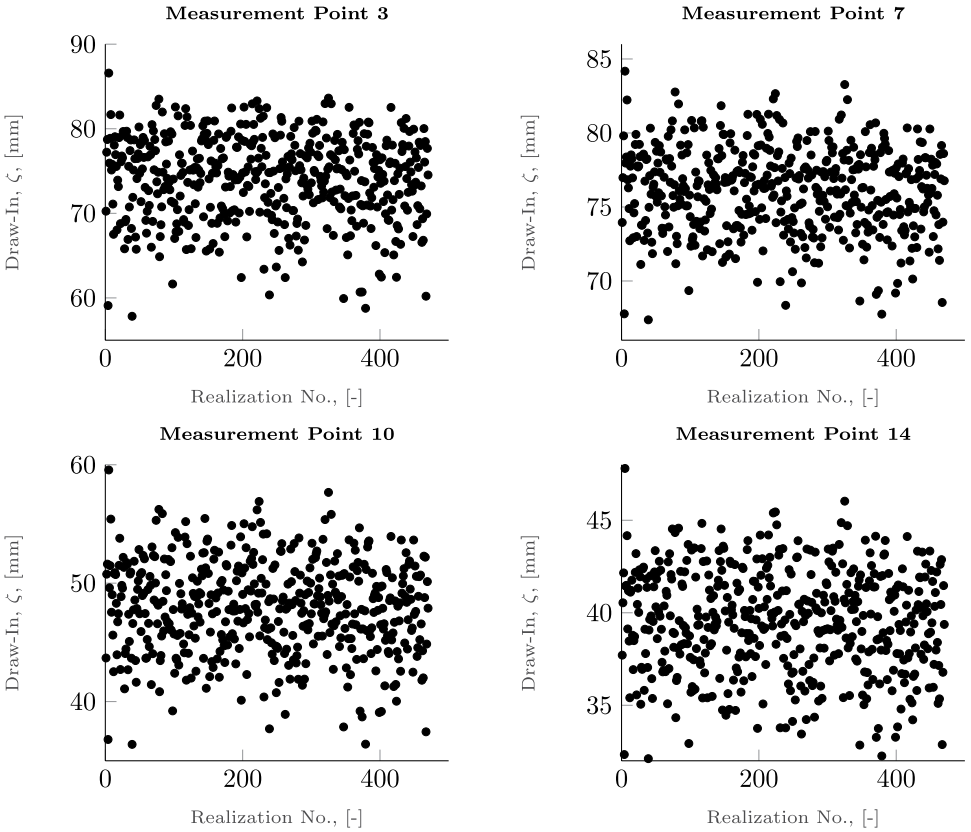

Fig. 14 Example of draw-in output from four measurement points

Input Layer

This layer comprises 19 neurons, corresponding to the number of input parameters. Input data is fed into the network through this layer.

Hidden Layers

Three hidden layers are employed to extract increasingly complex features from the input data.The neural network architecture, with 8 neurons in the first layer, 16 in the second, and 3 in the third, was chosen after multiple iterative experiments.

First Hidden Layer: The first hidden layer consists of eight neurons, all fully connected to the input layer. The rectified Linear Unit (ReLU) activation function is employed in this layer. This layer captures fundamental input features, providing a broad overview.

Second Hidden Layer: Utilizing the same activation function ReLu, second hidden layer consists of 16 neurons. This layer enhances the network's capacity to identify complex patterns.

Third Hidden Layer: The third hidden layer is more compact, containing only three neurons. This layer has been introduced to capture more abstract features in the input data, optimized for the dimensionality of the output, balancing accuracy with computational efficiency. Like the other layers, this layer is followed by a ReLU function.

Output Layer

A single neuron output layer, connected to the third hidden layer, is used for prediction. A linear activation function followed by a regression layer produces the final output.

This layered architecture iteratively extracts increasingly complex features from the input data, ultimately generating a prediction. The architecture of the network is illustrated in Fig. 15.

Hyperparameter Tuning

Key hyperparameters, including learning rate, batch size, and number of epochs, were optimized using grid search and cross-validation. This systematic tuning process

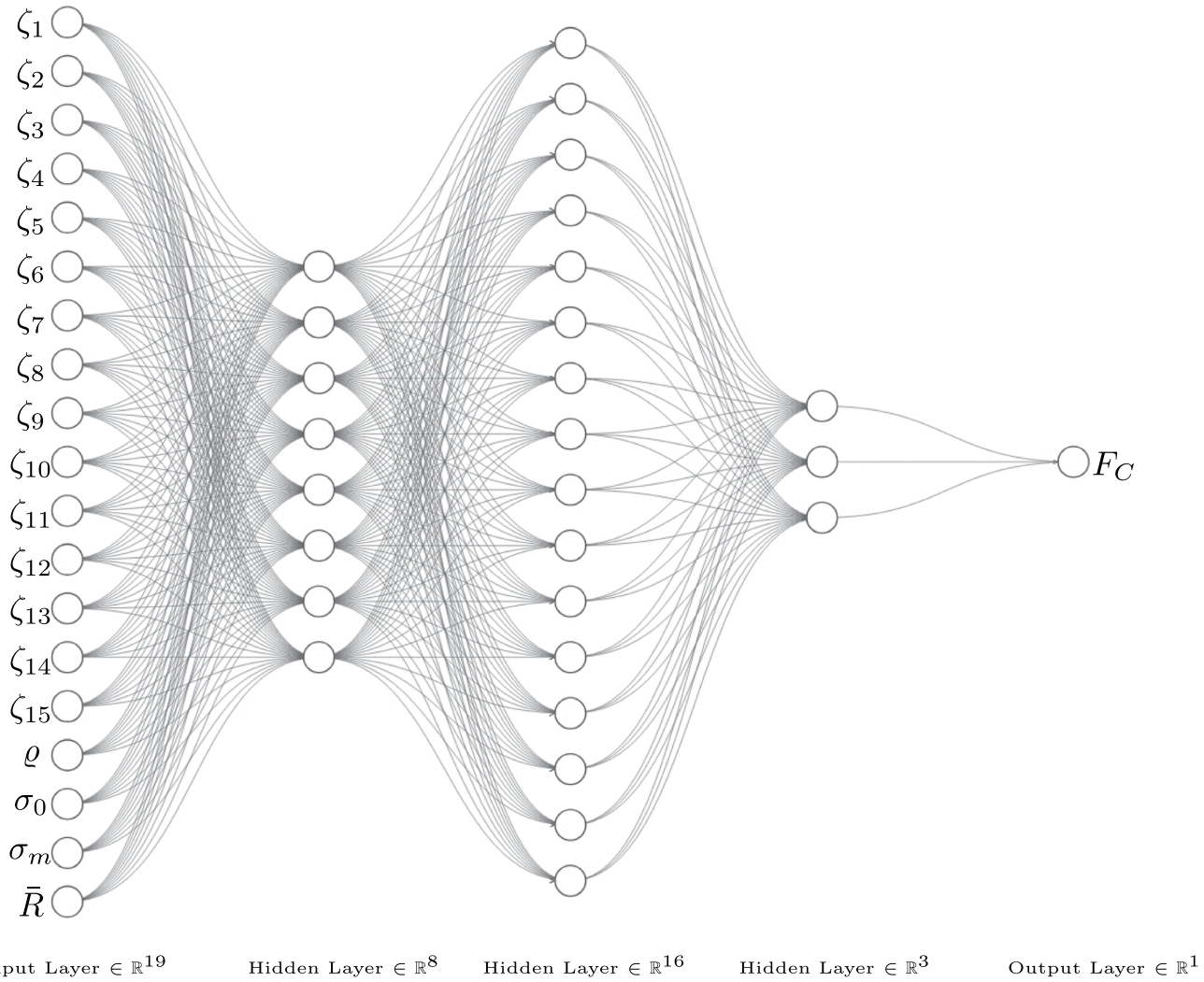

Fig. 15 Schematic of the developed artificial neural network architecture

ensured the model reached an optimal performance level without overfitting.

Alternative architectures with varying numbers of hidden layers and neurons were evaluated. Simpler models exhibited underfitting, while more complex networks led to overfitting. The selected configuration demonstrated the best trade-off between performance and generalization.

Data processing

Robust data pre-processing is essential for optimizing neural network performance. In this study, dataset inconsistencies primarily stemmed from outliers, mislabeled data, and NaN values from computational errors. Outliers were systematically detected using interquartile range (IQR) analysis, followed by careful manual review and removal to ensure data integrity.

To further enhance model learning, missing values were initially imputed with zeros to prevent computational errors during training. This choice was made due to the dataset's sparse nature, where zero values were less likely to introduce bias compared to mean or median imputation. Due to the large dataset size and the relatively small proportion of zero-imputed values, the overall performance of the neural network remained unaffected. The sparsity of zero imputations minimized any potential impact on the model's sensitivity to feature interactions.

To maintain consistency and ensure comparable scales among input features and output data, min-max normalization was applied.

Data splitting

To effectively train and evaluate the model, the dataset was randomly divided into training, validation, and testing subsets. This approach ensured the model learned from diverse data while its performance was assessed on unseen examples. By preventing overfitting, this strategy optimized model generalization and facilitated robust development and evaluation.

Training Set:

The training set comprises 73% of the total dataset and serves as the primary data source for the neural network's learning process. This subset is exposed to the model iteratively, allowing it to adjust its internal parameters (weights and biases) through backpropagation to minimize the prediction error. The goal is to establish robust patterns and correlations between the input features and the corresponding output data.

Validation Set:

Constituting 15% of the dataset, the validation set acts as a monitoring mechanism during the training process. It is crucial for preventing overfitting, a condition where the model becomes overly specialized to the training data and performs poorly on unseen data. By evaluating the model's performance on the validation set at regular intervals, hyperparameters (e.g., learning rate, number of epochs) can be adjusted to optimize generalization.

Testing Set:

The testing set, representing 12% of the dataset, is reserved for the final evaluation of the trained model. This set is entirely independent of the training and validation processes, ensuring an unbiased assessment of the model's predictive capabilities. This set follows the principle of "out-of-sample" validation. It offered insights into the model's predictive accuracy when applied to data that was not seen during the training and validation phases.

Network training

To optimize the neural network's learning process, the Adam optimizer was employed. This optimizers adaptive learning rate mechanism effectively navigates complex landscapes, such as those encountered with sparse gradients. For the given model a learning rate of 0.01 was used. The model was trained for a maximum of 297 epochs to ensure adequate exposure to the complex dataset. A mini-batch size of 64 samples was chosen to balance computational efficiency with performance gains. To prevent overfitting and monitor progress, the model's performance was evaluated every 10 iterations.

Implementation details

The model was implemented using MATLAB 2023b and trained on a personal computing system with sufficient computational resources to process the dataset efficiently. Given the dataset's large size, training was conducted using a high-performance CPU, ensuring stable performance and reasonable training times.

Out-of-sample evaluation and training performance

To evaluate the model's performance, standard evaluation metrics were utilized in the form of the Mean Squared Error (MSE) and R-squared (R^2) values. The MSE measures the average magnitude of prediction errors. It is a measure of the average squared difference between predicted and actual values. Lower MSE values indicate better predictive accuracy (Witten et al., 2011).

The R^2 quantifies the proportion of variance in the measurement points that is explained by the model. A higher R^2 indicates a better fit to the data (Kurz-Kim & Loretan, 2007).

Table 4 Configuration of the four experiments carried out at the Volvo Cars stamping plant in Olofström, Sweden

Measurement	σ_0 [MPa]	σ_m [MPa]	$\bar{R}$ [-]	ϱ [g/m^2]	F_C [kN]
M.1	147.9	290.7	2.03	1.00	1200
M.2	147.9	290.7	2.03	1.00	1500
M.3	147.9	290.7	2.03	1.00	1800
M.4	147.9	290.7	2.03	1.00	2000

The model was optimized to minimize the prediction errors, resulting in an MSE of 0.00052782305. This low MSE value indicates that the model has effectively learned the underlying patterns and relationships in the training data, reducing the average squared difference between the predicted and actual values. To provide a more interpretable error metric, the RMSE was calculated as 0.022974400. The small RMSE value confirms the model's high accuracy by quantifying the average prediction error in the same units as the output data, signifying very minimal deviations from the true values.

Industrial validation case

To evaluate the performance of the intelligent quality controller in an industrial environment, four physical experiments were carried out at the stamping facilities of Volvo Cars in Olofström, Sweden. All four experiments were performed on material from the same metal coil, why all experiments have recorded identical material parameters. Furthermore, to ensure control over the lubrication amount, the existing pre-lubrication was removed from the specimens and lubrication was added to a level of 1.00 [g/m^2]. To assess the performance of the developed neural network, the real time process parameter was varied to investigate the total defined solution space for the training data and beyond. The four values chosen for the experiments represents the minimum, average, and maximum values of the solution space as well as a value slightly outside the defined space. The configuration of the four experiments can be found in Table 4.

Draw-in measurements

The draw-in measurements of the four specimens was performed as a post-processing operation. The specimens were manually extracted from the press and a 3D scan was performed. For more information on the approach of 3D scanning and draw-in measurement this can be found in the paper published by Chezan et al. (2024). The draw-in measurements can be found in Fig. 16.

Industrial quality controller predictions

Providing the measured draw-in values to the neural network together with the material parameters and lubrication amount specified in Table 4, the network is able to provide a prediction of the correct cushion force which are presented in Fig. 17. The results provided by the neural network show the model performed exceptionally well in predicting three out of the four cushion force values, with RMSE values near zero (0.0001, 0.0003, and 0.0001 for measurement 1, 2, and 3 respectively), indicating near perfect predictions. The fourth prediction was however not accurately predicted - most likely due to the cushion force lying outside of the solution space defined for the training data. Therefore the presence of the imaginary component may reflect certain complexities or noise in the experimental data that the model could not fully capture.

Overall, the results indicate that the neural network model is highly effective in predicting cushion force values with minimal error, making it a reliable tool for applications requiring precise predictive modeling. The low training MSE and RMSE, combined with the near-perfect predictions on the experimental data, underscore the robustness and accuracy of the developed model.

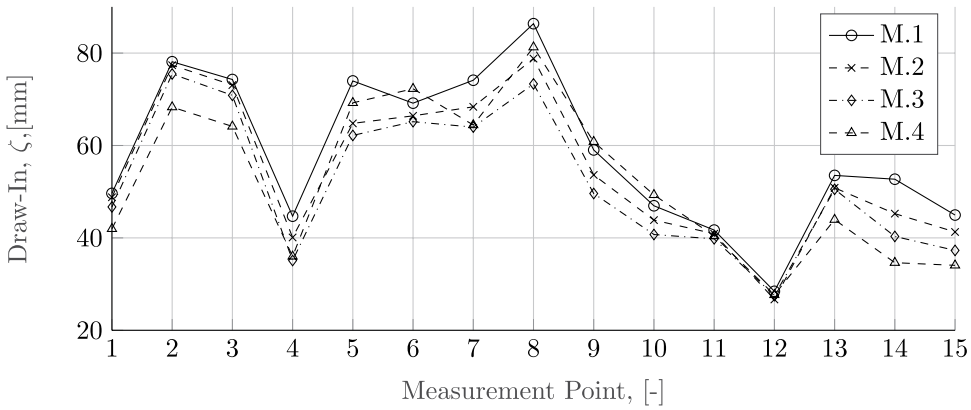

Fig. 16 Measured draw-in from the four experiments

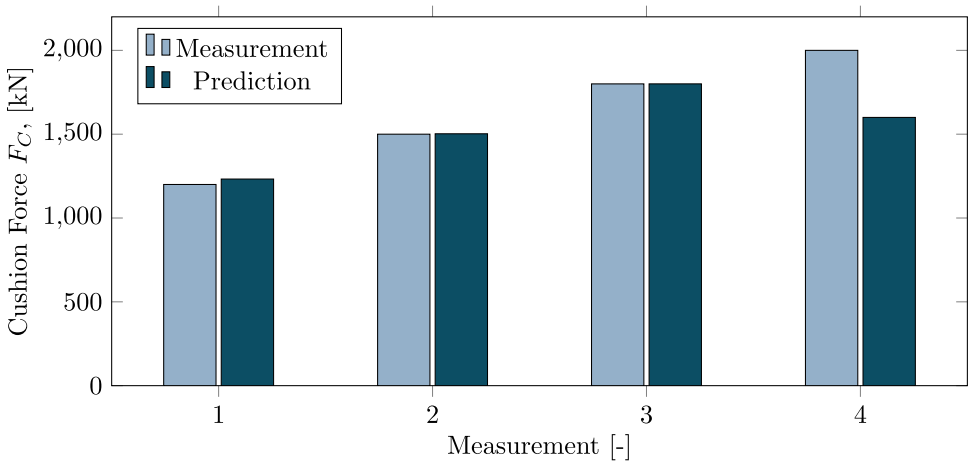

Fig. 17 Comparison of measured and predicted cushion force values for the four experiments

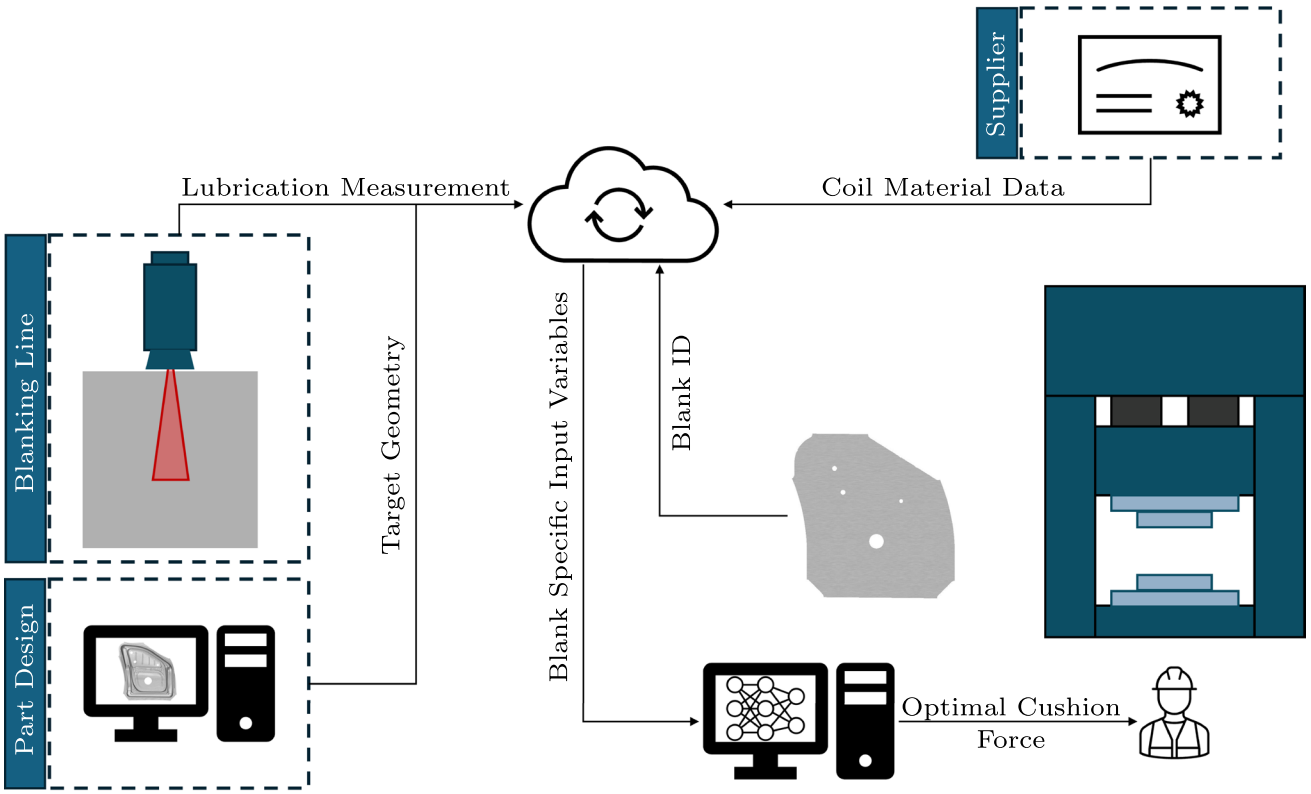

Fig. 18 "Illustration of the data flow in the proof-of-concept for operation support

Implementation

As outlined in Sect. 1.2 this study serves as a Proof-of-Concept (PoC) for the use of synthetic data for training purposes in an industrial setting. Therefore, a full implementation strategy for the controller with autonomous process parameter update will not be shown, but simply outlined.

In its current state, the ANN is however able to support operators on the production floor in making decisions based on the next-in-line blank going into the first forming stage of the press line. Figure 18 outlines the data flow between the data acquisition system outlined in Sect. 1.3, the ANN and the operator. In addition to the sensors and the information collected on the material properties of the suppliers, the geometry of the component in the nominal model is used as a target for the draw-in for the 15 draw-in points along the trapped blank.

One aspect of implementing a controller such as the one presented in this study, is operational trust. While the capabilities and potential of machine learning is well known and

understood in academic circles, the same knowledge is not necessarily present in industry. Currently, the modification of process parameters in the industrial testbed is based on operator experience. Therefore, the first stage of a full scale implementation is to show the operators that the developed controller would suggest similar or identical changes to the process as they would. Once the base level of trust of the controller has been established with the operator, the second stage is for the operators to actively include the controller in the decision making process as a support tool when running production batches. Lastly, the third stage of implementation, is once the controller is fully trusted and incorporated as a value adding support tool, only then can it be implemented as an autonomous control unit in the industrial testbed.

Conclusion and outlook

The findings of this study demonstrate how accurate numerical models can be build to generate training data for Artificial Neural Networks in an industrial environment, to predict events or outcomes in the physical domain. The study showed how a neural network with a feed-forward approach was able to predict experimentally measured values in three out of four industrial validation cases, with the failure in one case being attributed to the fact that the experimentally measured value was placed outside the solution space of the training data. While the proposed model demonstrates strong performance within the trained solution space, the authors acknowledge its limited generalization when applied to scenarios just outside the solution space. To address this limitation and improve the industrial robustness of the model, the authors propose the following strategy for extending the training space:

Variable sensitivity analysis: Perform a sensitivity analysis to identify the input parameters that most significantly affect model performance near the edges of the training domain. For the industrial demonstrator presented in this study, the cushion force would be the target for data generation.

Focused Simulation Expansion: Generate additional synthetic data in boundary regions using a targeted sampling method such as adaptive sampling, stratified sampling, or Latin hypercube designs. Given that simulations are fast and computationally inexpensive, this can be achieved efficiently.

Incremental model updating: Incorporate the new synthetic data into an updated training set and retrain the model iteratively. Cross-validation and performance benchmarking should be used throughout to monitor gains in generalization and prevent overfitting.

Simulation-guided domain expansion: This approach can be repeated in cycles, guided by model uncertainty or prediction error until an acceptable generalization is achieved across the expected process variability.

By leveraging the low-cost and flexible nature of numerical data generation, this strategy provides a scalable way to enhance the model's applicability across drifting process windows, without requiring real-world data collection or high computational overhead.

The use of numerically generated data for training intelligent systems is expected to open up the possibility for more manufacturers to use these systems, as it is faster and cheaper compared to training these systems on production data. Needed for the input to the intelligent systems is however a fully automated data acquisition (DAQ) system to measure e.g. lubrication amounts as well as mechanical parameters for every blank or every set length of metal coil.

Acknowledgements Open Access funding was provided by Blekinge Institute of Technology. This study was also funded by VINNOVA in the EUREKA Smart program (grant number 2021-03144).

Funding Open access funding provided by Blekinge Institute of Technology.

Data availability The dataset will be provided upon reasonable request.

Declarations

Conflict of interest The authors declare there are no conflict of interest associated to this study.

References

Abspoel, M., Scholting, M. E., Lansbergen, M., An, Y., & Vegter, H. (2017). A new method for predicting advanced yield criteria input parameters from mechanical properties. *Journal of Materials Processing Technology, 248*, 161–177. https://doi.org/10.1016/j.jmatprotec.2017.05.006

Amirgol, A. (2022). *Photogrammetry-based draw-in data acquisition for automotive part manufacturing process* (Unpublished master s thesis). Han University of Applied Sciences.

Atzema, E. H., Scholting, M. E., & Abspoel, M. (2021). Approaches to analysing scatter in forming simulations: From fundamental to

pragmatic. *IOP Conference Series: Materials Science and Engineering, 1157*, Article 012091. https://doi.org/10.1088/1757-899X/1157/1/012091

Banabic, D. (2010). *Sheet metal forming processes: Constitutive modelling and numerical simulation* (1st ed.). Springer.

Banabic, D., & Sester, M. (2012). Influence of material models on the accuracy of the sheet forming simulation. *Materials and Manufacturing Processes, 27*, 273–277. https://doi.org/10.1080/10426914.2011.578005273

Barlo, A., Aeddula, O., Chezan, T., Pilthammar, J., & Sigvant, M. (2024). Creating a virtual shadow of the manufacturing of automotive components. *IOP Conference Series: Materials Science and Engineering, 1307*, Article 012037. https://doi.org/10.1088/1757-899X/1307/1/012037

Barlo, A., Sigvant, M., & Pilthammar, J. (2024). Investigation of temperature impact on friction conditions in running production of automotive body components. *IOP Conference Series: Materials Science and Engineering, 1307*, Article 012004. https://doi.org/10.1088/1757-899X/1307/1/012004

Brun, M., Ghiotti, A., Bruschi, S., & Filippi, S. (2021). Active control of blankholder in sheet metal stamping. *Procedia CIRP, 100*, 151–156. https://doi.org/10.1016/j.procir.2021.05.079

Chezan, A. R., Atzema, E. H., Pilthammar, J., & Sigvant, M. (2023). Material variability effects on automotive part production process. *IOP Conference Series: Materials Science and Engineering, 1284*, Article 012037. https://doi.org/10.1088/1757-899X/1284/1/012037

Chezan, A. R., Dhawale, T., Atzema, E. H., Barlo, A., Aeddula, O., Pilthammar, J., & Langerak, N. A. J. (2024). Optimizing reverse-engineered finite element models for accurate predictions of experimental measurements. *IOP Conference Series: Materials Science and Engineering, 1307*, Article 012040. https://doi.org/10.1088/1757-899X/1307/1/012040

Chinnam, R. B., & Kolarik, W. J. (1997). Neural network-based quality controllers for manufacturing systems. *International Journal of Production Research, 35*(9), 2601–2620.

DIN 8582: Manufacturing processes forming - Classification; Subdivision, terms and definitions, alphabetical index (Vol. 2023; Standard). (2003). DEDeutsches Institut für Normung.

Gou, Y., Wang, C., Han, S., Kosec, G., Zhou, Y., Wang, L., & Wahab, M. A. (2025). A deep neural network model for parameter identificaiton in deep drawing metal forming process. *Journal of Manufacturing Processes, 133*, 380–394. https://doi.org/10.1016/j.jmapro.2024.11.067

Guo, P., & Yu, J. (2019). Optimal control of blank holder force based on deep reinforcement learning. In *2019 IEEE international conference on industrial engineering and engineering management (IEEM)* (pp. 1466–1470).

Hol, J., Cid Alfaro, M. V., de Rooij, M. B., & Meinders, T. (2012). Advanced friction modelling for sheet metal forming. *Wear, 286–287*, 66–78. https://doi.org/10.1016/j.wear.2011.04.004

Hol, J., Wiebenga, J. H., & Carleer, B. (2017). Friction and lubrication modelling in sheet metal forming: Influence of lubrication amount, tool roughness and sheet coating on product quality. *Journal of Physics: Conference Series, 896*, Article 012026. https://doi.org/10.1088/1742-6596/896/1/012026

Hosford, W.F., & Caddell, R.M. (2007). *Metal forming: Mechanics and metallurgy* (3rd ed.). Cambridge University Press.

Hou, C. K. J., & Behdinan, K. (2025). Neural networks with dimensionality reduction for efficient springback prediction in deep drawing of multi-material cylindrical cups. *Journal of Experimental & Theoretical Artificial Intelligence, 37*, 111–130. https://doi.org/10.1080/0952813X.2023.2183271

Jeong, Y., Singh, A., Zafarzadeh, M., Wiktorsson, M., & Baalsrud Hauge, J. (2020). Data-driven manufacturing simulation: Towards a cps-based approach. *Proceedings of the Swedish Production Symposium, 13*, 586–596.

Kott, M., Erz, C., Heingärtner, J., & Groche, P. (2020). Controllability of temperature induced friction effects during deep drawing of car body parts with high drawing depths in series production. *Procedia Manufacturing, 47*, 553–560. https://doi.org/10.1016/j.promfg.2020.04.166

Kurz-Kim, J- R., & Loretan, M. (2007). A note on the coefficient of determination in models with infinite variance variables. In *FRB International Finance Discussion Paper*, (895), https://doi.org/10.2139/ssrn.996664

Lehrer, T., Kaps, A., Lepenies, I., Duddeck, F., & Wagner, M. (2023). 2s-ml: A simulation-based classification and regression approach for drawability assessment in deep drawing. *International Journal of Material Forming*, *16*(56), https://doi.org/10.1007/s12289-023-01770-3

Link, P., Penter, L., Rückert, U., Klingel, L., Verl, A., & Ihlenfeldt, S. (2025). Real-time quality prediction and local adjustment of friction with digital twin in sheet metal forming. *Robotics and Computer-Integrated Manufacturing, 91*, Article 102848. https://doi.org/10.1016/j.rcim.2024.102848

Maier, L., Ünver, B., Volk, W., & Hartmann, C. (2024). Simulation-based data reduction and data processing for sheet metal forming in the hybrid twin framwork. *International Journal of Advanced Manufacturing Technology*. https://doi.org/10.1007/s00170-024-14135-0

Maier, S., Liebig, A., Kautz, T., & Volk, W. (2017). Tool-integrated spring back measuring system for automotive press shop: A contribution to the quality control of complex car body parts. *Production Engineering, 11*, 307–313. https://doi.org/10.1007/s11740-017-0725-8

Morand, L., Helm, D., Iza-Teran, R., & Garcke, J. (2019). A knowledge-based surrogate modeling approach for cup drawing with limited data. *IOP Conference Series: Materials Science and Engineering,651*. https://doi.org/10.1088/1757-899X/651/1/012047

Muñiz, L., Trinidad, J., Garcia, E., Peinado, I., Montes, N., & Galdos, L. (2023). On the use of advanced friction models for the simulation of an industrial stamping process including the analysis of material and lubrication fluctuations. *Lubricants, 11*, 193. https://doi.org/10.3390/lubricants11050193

Pareek, K. A., May, D., Meszmer, P., Ras, M. A., & Wunderle, B. (2025). Synthetic data generation usning finite element method to pre-train an image segmentation model for defect detection using infrared thermography. *Journal of Intelligent Manufacturing, 36*, 1879–1905. https://doi.org/10.1007/s10845-024-02326-1

Pilthammar, J. (2020). *Towards virtual tryout and digital twins: Enhanced modelling of elastic dies, sheet materials, and friction in sheet metal forming* (Unpublished doctoral dissertation). Blekinge Institute of Technology.

Pilthammar, J., Banabic, D., & Sigvant, M. (2021). Bbc 2005 with non-integer exponent and ambiguities in nakajima yield surface calibration. *International Journal of Material Forming, 14*, 577–592. https://doi.org/10.1007/s12289-020-01545-0

Pilthammar, J., Schill, M., Sigvant, M., Sjöblom, V., & Lind, M. (2019). Simulation of sheet metal forming using elastic stamping dies. In *Proceedings of the 12th european ls-dyna conference 2019, koblenz, germany.*

Pilthammar, J., Sigvant, M., & Kao-Walter, S. (2018). Introduction of elastic die deformations in sheet metal forming simulations. *International Journal of Solids and Structures, 151*, 76–90. https://doi.org/10.1016/j.ijsolstr.2017.05.009

Sbaragli, A., Ghafoorpoor, P. Y., Thiede, S., & Iati, F. (2025). A cyber-physical architecture to monitor human-centrcic reconfigurable manufacturing systems. *Journal of Intelligent Manufacturing*. https://doi.org/10.1007/s10845-024-02558-1

Semeraro, C., Lezoche, M., Panetto, H., & Dassisti, M. (2021). Digital twin paradigme: A systematic literature review. *Computers in Industry, 130*, Article 103469. https://doi.org/10.1016/j.compind.2021.103469

Sigvant, M., & Carleer, B. (2006). Influence on simulation results from material and process scatter. In *Proceedings of the iddrg 2006 conference, porto, portugal.*

Sigvant, M., Pilthammar, J., Hol, J., Wiebenga, J. H., Chezan, T., Carleer, B., & van den Boogaard, A. H. (2016). Friction and lubrication modeling in sheet metal forming simulations of a volvo xc90 inner door. *IOP Conference Series: Materials Science and Engineering, 159*, Article 012021. https://doi.org/10.1088/1757-899X/159/1/012021

Sigvant, M., Pilthammar, J., Hol, J., Wiebenga, J. H., Chezan, T., Carleer, B., & van den Boogaard, T. (2019). Friction in sheet metal forming: Influence of surface roughness and strain rate on sheet metal forming simulation results. *Procedia Manufacturing, 29*, 512–519. https://doi.org/10.1016/j.promfg.2019.02.169

Sigvant, M., Pilthammar, J., Tatipala, S., & Andreasson, E. (2018). Smart stamping: Improved quality in stamping by model driven control. In*Proceedings of the 11th forming technology forum conference, Zurich, Switzerland*.

Simonetto, E., Ghiotti, A., Brun, M., Bruschi, S., & Filippi, S. (2023). Adaptive metal flow control in stamping through ferrofluidic actuators. *CIRP Annals, 72*, 209–212. https://doi.org/10.1016/j.cirp.2023.03.030

Singer, G., & Cohen, Y. (2021). A framework for smart control using machine-learning modeling for processes with closed loop control in industry 4.0. *Engineering Applications of Artificial Intelligence, 103*, Article 104236. https://doi.org/10.1016/j.engappai.2021.104236

Smolic, H. (2024). *How much data do you need for machine learning.* https://graphite-note.com/how-much-data-is-needed-for-machine-learning/. (Accessed: 22.08.2024)

Tao, F., Qi, Q., Liu, A., & Kusiak, A. (2018). Data-driven smart manufacturing. *Journal of Manufacturing Systems, 48*, 157–169. https://doi.org/10.1016/j.jmsy.2018.01.006

TATA Steel Europe (2025). *Aurora®, online.* https://www.tatasteeleurope.com/automotive/aurora-online

Tatipala, S., Pilthammar, J., Sigvant, M., Wall, J., & Johansson, C. M. (2018). Introductory study of sheet metal forming simulations to evaluate process robustness. *IOP Conference Series: Materials Science and Engineering, 418*, Article 012111. https://doi.org/10.1088/1757-899X/418/1/012111

Tatipala, S., Wall, J., Johansson, C. M., & Sigvant, M. (2018). Data-driven modelling in the era of industry 4.0: A case study of friction modelling in sheet metal forming simulations. *Journal of Physics: Conference Series, 1063*, Article 012135. https://doi.org/10.1088/1742-6596/1063/1/012135

Thiery, S., Abdine, M. Z. E., Heger, J., & Khalifa, N. B. (2024). Neural network-based eistimation and compensation of friction for enhanced deep drawing process control. *Materials Research Proceedings, 41*, 1462–1471.

Tommerup, S., & Endelt, B. (2012). Experimental verification of a deep drawing tool system for adaptive blank holder pressure distribution. *Journal of Materials Processing Technology, 212*, 2529–2540. https://doi.org/10.1016/j.jmatprotec.2012.06.015

Tricarico, L., & Palmieri, M. E. (2023). Robust design of deep drawing process through in-line feedback control of the draw-in. *Applied Sciences, 13*(3), 1717. https://doi.org/10.3390/app13031717

Verband der Automobilindustrie (2024). *Vda239-100: Sheet steel for cold forming.* https://webshop.vda.de/VDA/en/vda-239-100-052024.

Waanders, D., Hazrati, J., Kott, M., Gastebois, S., & Hol, J. (2020). Temperature dependent friction modelling: The influence of temperature on product quality. *Procedia Manufacturing, 47*, 535–540. https://doi.org/10.1016/j.promfg.2020.04.159

Witten, I.H., Frank, E., Hell, M.A. (2011). *Data mining: Practical machine learning tools and techniques* (3rd ed.). Elsevier Inc.

Wollschlaeger, L., Heinzel, C., Thiery, S., Abdine, M. Z. E., Khalifa, N. B., & Heger, J. (2024). Increased reliability of draw-in prediciton in a single stage deep-drawing operation via transfer learning. *Procedia CIRP,130*. https://doi.org/10.1016/j.procir.2024.10.086

Yu, F., & Nielsen, C. P. (2020). A data-driven approach for decision-making support of factory simulation solutions. *Procedia CIRP, 93*, 971–976. https://doi.org/10.1016/j.procir.2020.04.129